Inorganic Chemistry

Article

pubs.acs.org/IC

# Ternary Arsenides $A_2Zn_5As_4$ (A = K, Rb): Zintl Phases Built from *Stellae Quadrangulae*

Stanislav S. Stoyko, Mansura Khatun, and Arthur Mar*

Department of Chemistry, University of Alberta, Edmonton, Alberta, Canada T6G 2G2

Supporting Information

**ABSTRACT:** Stoichiometric reaction of the elements at high temperature yields the ternary arsenides $K_2Zn_5As_4$ (650 °C) and $Rb_2Zn_5As_4$ (600 °C). They adopt a new structure type (Pearson symbol *oC*44, space group *Cmcm*, $Z = 4$; $a = 11.5758(5)$ Å, $b = 7.0476(3)$ Å, $c = 11.6352(5)$ Å for $K_2Zn_5As_4$; $a = 11.6649(5)$ Å, $b = 7.0953(3)$ Å, $c = 11.7585(5)$ Å for $Rb_2Zn_5As_4$) with a complex three-dimensional framework of linked $ZnAs_4$ tetrahedra generating large channels that are occupied by the alkali-metal cations. An alternative and useful way of describing the structure is through the use of *stellae quadrangulae* each consisting of four $ZnAs_4$ tetrahedra capping an empty central tetrahedron. These compounds are Zintl phases; band structure calculations on $K_2Zn_5As_4$ and $Rb_2Zn_5As_4$ indicate semiconducting behavior with a direct band gap of 0.4 eV.

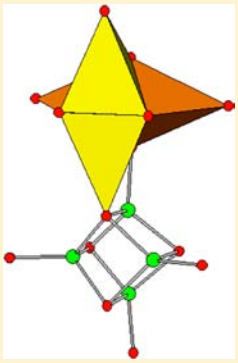

## INTRODUCTION

Much of the current resurgence of interest in ternary arsenides A−M−As containing an electropositive metal A and a transition metal M can be traced to the discovery of useful materials properties, particularly superconductivity in $BaFe_2As_2$ and related compounds.[1] However, these arsenides are significant in their own right for their diverse structural chemistry, originating from the different ways that heteronuclear anionic units $MAs_n$ can be linked to form complex extended frameworks; for the most part, they can be considered to be Zintl phases.[2] Given previous work on ternary rare-earth-metal zinc arsenides RE−Zn−As,[3−5] we and others have been interested in extending these studies to systems containing other electropositive components, such as alkaline-earth metals.[6−9] The alkali-metal-containing systems A−Zn−As remain sparsely investigated, and examples of compounds have been so far limited to a few: LiZnAs (MgAgAs-type),[10−13] NaZnAs (MgAgAs- and PbFCl-types),[14−16] KZnAs (ZrBeSi- and LiBaSi-types),[15,17] $NaZn_4As_3$ ($RbCd_4As_3$-type),[18] $AZn_4As_3$ (A = K, Rb, Cs; $KCu_4S_3$-type),[18] and $K_4ZnAs_2$ ($K_4CdP_2$-type).[19] LiZnAs has been identified as a host material that can be doped to induce ferromagnetism.[20]

Herein we report the preparation of the ternary arsenides $K_2Zn_5As_4$ and $Rb_2Zn_5As_4$. They adopt a new and unusual structure type which can be described through *stellae quadrangulae* as the building units. Their relationships to other structures are drawn, and the bonding in these Zintl phases is examined through the use of band structure calculations.

## EXPERIMENTAL SECTION

**Synthesis.** Starting materials were K pieces (99.95%, Alfa-Aesar), Rb pieces (99.75%, Alfa-Aesar), Zn shot (99.99%, Aldrich), and As lumps (99.999%, Alfa-Aesar). All reagents and products were handled within an argon-filled glovebox. Stoichiometric mixtures of the elements were loaded into alumina crucibles placed within fused-silica tubes, which were evacuated and sealed. The tubes were heated to 650 °C (for K samples) or 600 °C (for Rb samples) over 2 d, held at that temperature for 10 d, and cooled to room temperature over 2 d. The use of a lower annealing temperature for the Rb samples was prompted by the low boiling point for Rb metal (688 °C). Products were analyzed by powder X-ray diffraction (XRD) on an Inel diffractometer equipped with a curved position-sensitive detector (CPS 120) and a Cu $K\alpha_1$ radiation source operated at 40 kV and 20 mA. The powder XRD patterns revealed that the K-containing reactions gave nearly quantitative yields of $K_2Zn_5As_4$ along with small amounts (less than 5%) of KZnAs, whereas the Rb-containing reactions gave nearly equal proportions of $Rb_2Zn_5As_4$ and $RbZn_4As_3$ (Figure S1 in Supporting Information). The lower yields for $Rb_2Zn_5As_4$ are likely associated with partial evaporative loss of Rb metal from the open alumina crucibles and reaction with the fused-silica tubes. However, an alternative explanation for the differences in the reaction products for the K- versus Rb-containing reactions is that the ternary compounds, once formed, may be prone to undergo decomposition at high temperature. Single crystals of the title compounds are moderately air-sensitive, although they can be handled without any special precautions for several minutes before tarnishing. Crystals were selected under paraffin oil and examined by energy-dispersive X-ray (EDX) analysis on a JEOL JSM-6010LA scanning electron microscope. A representative SEM image is shown in Figure S2 in Supporting Information. The experimentally determined average compositions (in atomic %) were $K_{19(2)}Zn_{44(1)}As_{37(2)}$ and $Rb_{20(2)}Zn_{45(1)}As_{35(2)}$, which are in excellent agreement with expectations ($A_{18.2}Zn_{45.4}As_{36.4}$). Attempts were made to prepare the Na analogue of these compounds, under similar conditions as above, to no avail. Reactions with Cs were not attempted.

**Structure Determination.** Suitable single crystals were mounted within small droplets of paraffin oil on glass fibers and placed under a cold nitrogen gas stream on a Bruker D8 ($K_2Zn_5As_4$) or a Bruker

**Received:** June 20, 2012
**Published:** August 17, 2012

   dx.doi.org/10.1021/ic301311m | *Inorg. Chem.* 2012, 51, 9517−9521

PLATFORM ($Rb_2Zn_5As_4$) diffractometer, each equipped with a SMART APEX II CCD detector and a Mo K$\alpha$ radiation source. Full spheres of intensity data were collected at −100 °C using $\omega$ scans with a scan width of 0.3° and an exposure time of 15 s per frame in 7 ($K_2Zn_5As_4$) or 5 ($Rb_2Zn_5As_4$) batches. Face-indexed numerical absorption corrections were applied. Structure solution and refinement were carried out with use of the SHEXTL (version 6.12) program package.[21] Crystal data and further experimental details are given in Table 1. The centrosymmetric orthorhombic space group *Cmcm* was chosen on the basis of the Laue symmetry, systematic absences, and intensity statistics (mean $|E^2 - 1|$ of 0.920 for $K_2Zn_5As_4$ and 0.969 for $Rb_2Zn_5As_4$). Initial atomic positions were easily located by direct methods, and refinements proceeded in a straightforward manner. All sites are fully occupied and have reasonable displacement parameters. Atomic positions were standardized with the program STRUCTURE TIDY.[22] Final values of the positional and displacement parameters are given in Table 2, and selected interatomic distances are listed in Table 3.

**Table 1. Crystallographic Data for $A_2Zn_5As_4$ (A = K, Rb)**

| formula | $K_2Zn_5As_4$ | $Rb_2Zn_5As_4$ |
|---|---|---|
| formula mass (amu) | 704.73 | 797.47 |
| space group | *Cmcm* (No. 63) | *Cmcm* (No. 63) |
| $a$ (Å) | 11.5758(5) | 11.6649(5) |
| $b$ (Å) | 7.0476(3) | 7.0953(3) |
| $c$ (Å) | 11.6352(5) | 11.7585(5) |
| $V$ (Å$^3$) | 949.22(7) | 973.20(7) |
| $Z$ | 4 | 4 |
| $\rho_{calcd}$ (g cm$^{-3}$) | 4.931 | 5.443 |
| $T$ (K) | 173(2) | 173(2) |
| crystal dimensions (mm$^3$) | 0.07 × 0.16 × 0.21 | 0.04 × 0.08 × 0.09 |
| radiation | graphite-monochromated Mo K$\alpha$, $\lambda$ = 0.710 73 Å | |
| $\mu$(Mo K$\alpha$) (mm$^{-1}$) | 27.09 | 35.50 |
| transmission factors | 0.032−0.264 | 0.134−0.386 |
| 2$\theta$ limits | 6.76−66.32° | 6.72−66.46° |
| data collected | $-17 \le h \le 17$ | $-17 \le h \le 17$ |
| | $-10 \le k \le 10$ | $-10 \le k \le 10$ |
| | $-17 \le l \le 17$ | $-17 \le l \le 18$ |
| no. data collected | 6481 | 6610 |
| no. unique data, including $F_o^2 < 0$ | 981 ($R_{int}$ = 0.018) | 1004 ($R_{int}$ = 0.031) |
| no. unique data, with $F_o^2 > 2\sigma(F_o^2)$ | 948 | 905 |
| no. variables | 35 | 35 |
| $R(F)$ for $F_o^2 > 2\sigma(F_o^2)$[a] | 0.014 | 0.016 |
| $R_w(F_o^2)$[b] | 0.032 | 0.034 |
| GOF | 1.28 | 1.08 |
| $(\Delta\rho)_{max}$, $(\Delta\rho)_{min}$ (e Å$^{-3}$) | 0.77, −0.61 | 0.93, −0.70 |

[a] $R(F) = \sum||F_o| - |F_c||/\sum|F_o|$. [b] $R_w(F_o^2) = [\sum[w(F_o^2 - F_c^2)^2]/\sum wF_o^4]^{1/2}$; $w^{-1} = [\sigma^2(F_o^2) + (Ap)^2 + Bp]$, where $p = [\max(F_o^2,0) + 2F_c^2]/3$.

**Table 3. Selected Interatomic Distances (Å) in $A_2Zn_5As_4$ (A = K, Rb)**

| | $K_2Zn_4As_4$ | $Rb_2Zn_5As_4$ |
|---|---|---|
| A−As2 (×2) | 3.3485(4) | 3.4219(3) |
| A−As1 (×2) | 3.4346(2) | 3.4798(2) |
| A−As1 (×2) | 3.7312(2) | 3.7576(2) |
| A−As2 (×2) | 3.8377(4) | 3.8280(3) |
| A−Zn1 (×2) | 3.4379(3) | 3.4576(2) |
| A−Zn2 (×2) | 3.6966(5) | 3.6976(3) |
| A−Zn2 (×2) | 3.7102(4) | 3.7560(3) |
| A−Zn3 (×2) | 3.8253(3) | 3.8852(2) |
| A−Zn1 (×2) | 4.0680(2) | 4.0973(3) |
| A−A (×2) | 3.6181(3) | 3.6268(2) |
| Zn1−As1 | 2.4682(3) | 2.4963(4) |
| Zn1−As2 (×2) | 2.5497(2) | 2.5515(3) |
| Zn1−As1 | 2.6256(3) | 2.6592(5) |
| Zn2−As2 | 2.4535(3) | 2.4846(4) |
| Zn2−As1 (×2) | 2.5743(2) | 2.5778(3) |
| Zn2−As2 | 2.6636(3) | 2.6648(5) |
| Zn3−As1 (×2) | 2.5437(3) | 2.5605(5) |
| Zn3−As2 (×2) | 2.5848(3) | 2.6088(5) |
| Zn1−Zn2 (×2) | 2.9961(3) | 3.0411(4) |
| Zn2−Zn3 (×2) | 2.9977(4) | 3.0228(6) |
| Zn1−Zn3 | 3.1387(4) | 3.1327(6) |

Further data, in the form of crystallographic information files (CIFs), are available as Supporting Information or may be obtained from Fachinformationszentrum Karlsruhe, Abt. PROKA, 76344 Eggenstein-Leopoldshafen, Germany (CSD-424848 to 424849).

**Band Structure Calculations.** Tight-binding linear muffin tin orbital band structure calculations were performed on $K_2Zn_5As_4$ within the local density and atomic spheres approximation with use of the Stuttgart TB-LMTO-ASA program (version 4.7).[23] The basis sets included K 4s/4p/3d, Zn 4s/4p/3d, and As 4s/4p/4d orbitals, with the K 4p/3d and As 4d orbitals being downfolded. The unit cell contains two formula units. Calculations were performed with an increasing number of $k$ points (ranging from 172 to 666 within the first Brillouin zone) until the total energy did not deviate by more than $10^{-5}$ eV/cell. Integrations in

**Table 2. Atomic Coordinates and Equivalent Isotropic Displacement Parameters for $A_2Zn_5As_4$ (A = K, Rb)**

| atom | Wyckoff position | $x$ | $y$ | $z$ | $U_{eq}$ (Å$^2$)[a] |
|---|---|---|---|---|---|
| $K_2Zn_5As_4$ | | | | | |
| K | 8*e* | 0.214 56(4) | 0 | 0 | 0.013 31(9) |
| Zn1 | 8*g* | 0.143 14(2) | 0.386 09(4) | 1/4 | 0.009 68(6) |
| Zn2 | 8*f* | 0 | 0.652 36(4) | 0.108 52(2) | 0.010 13(6) |
| Zn3 | 4*c* | 0 | 0.007 84(5) | 1/4 | 0.010 72(8) |
| As1 | 8*g* | 0.341 53(2) | 0.257 79(3) | 1/4 | 0.007 56(6) |
| As2 | 8*f* | 0 | 0.274 84(3) | 0.097 69(2) | 0.007 59(6) |
| $Rb_2Zn_5As_4$ | | | | | |
| Rb | 8*e* | 0.217 69(2) | 0 | 0 | 0.010 61(7) |
| Zn1 | 8*g* | 0.143 35(3) | 0.383 26(5) | 1/4 | 0.009 81(8) |
| Zn2 | 8*f* | 0 | 0.654 03(5) | 0.108 68(3) | 0.009 88(8) |
| Zn3 | 4*c* | 0 | 0.009 91(7) | 1/4 | 0.010 91(10) |
| As1 | 8*g* | 0.343 19(2) | 0.257 39(4) | 1/4 | 0.007 29(7) |
| As2 | 8*f* | 0 | 0.278 83(4) | 0.098 70(2) | 0.007 30(7) |

[a] $U_{eq}$ is defined as one-third of the trace of the orthogonalized $U_{ij}$ tensor.


dx.doi.org/10.1021/ic301311m | *Inorg. Chem.* 2012, 51, 9517−9521

reciprocal space were carried out with an improved tetrahedron method over 666 irreducible $k$ points within the first Brillouin zone. A similar calculation was conducted on $Rb_2Zn_5As_4$ to investigate how the band gap is influenced by a change in the alkali-metal substituent.

## RESULTS AND DISCUSSION

The preparation of the new arsenides $A_2Zn_5As_4$ (A = K, Rb) illustrates the richness of these ternary A–Zn–As systems.

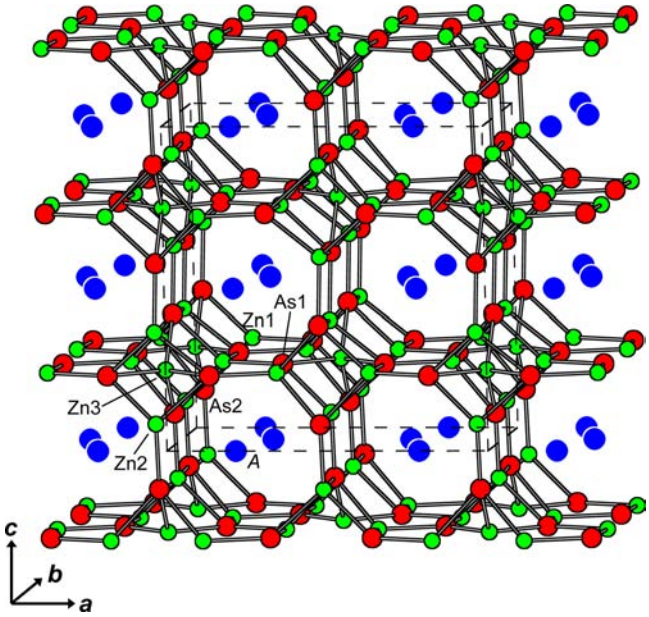


**Figure 1.** Structure of $A_2Zn_5As_4$ (A = K, Rb), viewed approximately down the $b$-direction, in a ball-and-stick representation. The large blue circles are A atoms, the small green circles are Zn atoms, and the medium red circles are As atoms.

All known phases to date can be considered to be members of the pseudobinary join $A_3As–Zn_3As_2$: $A_4ZnAs_2$ ($^4/_3$ $A_3As$ + $^1/_3$ $Zn_3As_2$),[19] AZnAs ($^1/_3$ $A_3As$ + $^1/_3$ $Zn_3As_2$),[10−17] $A_2Zn_5As_4$ ($^2/_3$ $A_3As$ + $^5/_3$ $Zn_3As_2$), and $AZn_4As_3$ ($^1/_3$ $A_3As$ + $^4/_3$ $Zn_3As_2$).[18] This pattern reflects their shared features of being Zintl phases with structures built up from simple Zn-centered polyhedra and having no homoatomic As–As bonds. There are recent reports that analogous Cd-containing arsenides and antimonides isostructural to $A_2Zn_5As_4$ can also be formed: $Rb_2Cd_5As_4$,[18] $Rb_2Cd_5Sb_4$,[24] and $Cs_2Cd_5Sb_4$.[24,25]

The structure type (space group *Cmcm*, Pearson symbol *oC*44, Wyckoff sequence *g*2 *f*2 *e c*) is new. $ZnAs_4$ tetrahedra are linked through corner- and edge-sharing to form a three-dimensional framework, generating large channels extending along the *b*-direction within which lie the A atoms (Figure 1). Because the connectivity of the $ZnAs_4$ tetrahedra is a little difficult to visualize in a conventional ball-and-stick drawing, it is helpful to switch to a polyhedral representation (Figure 2). Now it becomes evident that two types of tetrahedra (centered by Zn1 and Zn2) are arranged in an interesting way to form a unit called a *stella quadrangula* (also tetrahedral star or tetraederstern), basically a tetracapped tetrahedron. Such units can be useful for describing complex crystal structures as diverse as silicates and alloys.[26−30] Here, two Zn1- and two Zn2-centered tetrahedra form the caps of these units, leaving the central tetrahedron empty. Another way to view this unit is as a heterocubane structure, with $Zn_4As_4$ as the central cube and additional As atoms attached to four corners. The *stellae* are extended along the *c*-direction through edge-sharing, and within the *ab*-plane through corner-sharing. The third type of tetrahedra (centered by Zn3 atoms) also serve to link these units within the *ab*-plane through edge-sharing. Although the presence of A cations enclosed in large 20-vertex coordination polyhedra (Figure 3) suggests some resemblance to clathrate

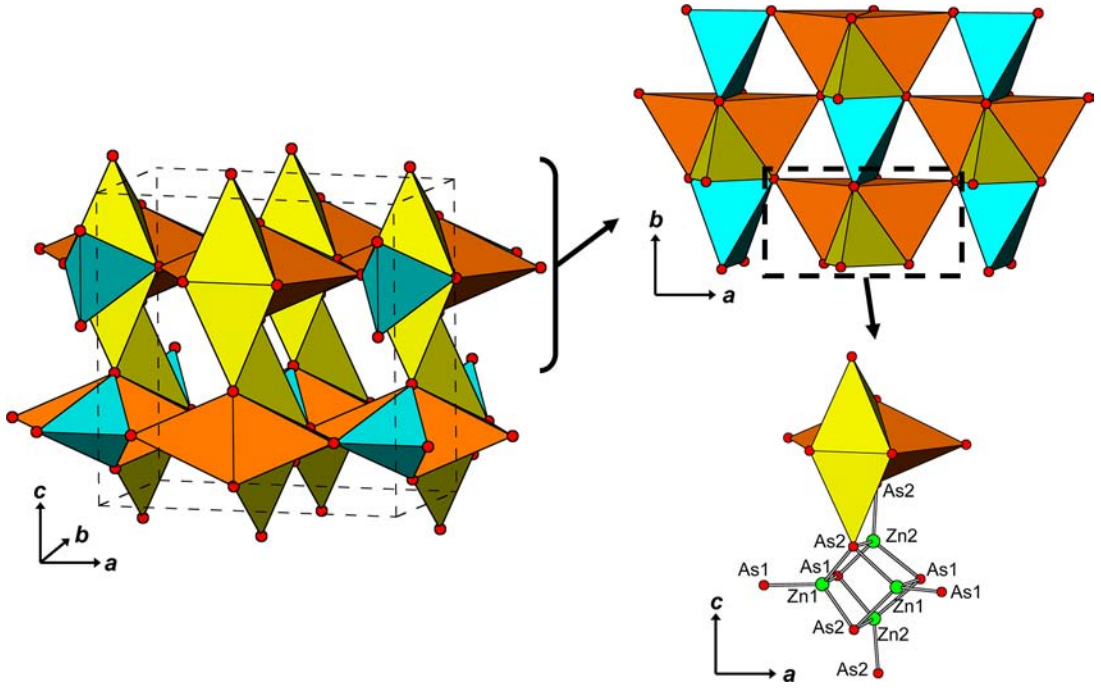


**Figure 2.** With the A atoms omitted for clarity, the 3D-framework of $A_2Zn_5As_4$ (A = K, Rb) can be built up from $ZnAs_4$ tetrahedra. Two Zn1- (orange) and two Zn2-centered tetrahedra (yellow) are connected to form a *stella quadrangula*; these units are further linked by Zn3-centered tetrahedra (cyan).


dx.doi.org/10.1021/ic301311m | *Inorg. Chem.* 2012, 51, 9517–9521

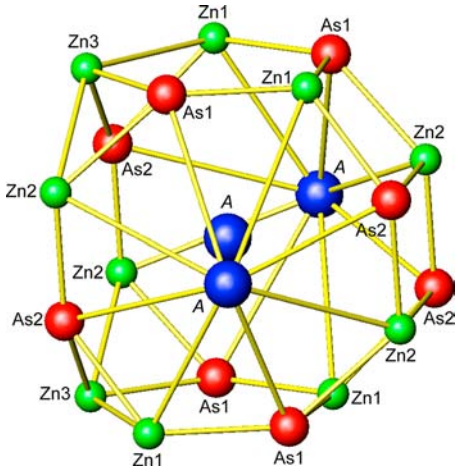


**Figure 3.** Coordination environment around an A atom in $A_2Zn_5As_4$ (A = K, Rb), forming a 20-vertex polyhedron.

structures of related antimonides,[24,25] these polyhedra are highly irregular and they interpenetrate each other along the *b*-direction. A more distant relationship that can be drawn is to $K_2Cu_2Te_5$, which has similar cell parameters and almost the same Wyckoff sequence as $A_2Zn_5As_4$ except that an 8*f* site is missing.[31] Both contain flat nets parallel to the *ab*-plane with similar topologies but different patterns of metal and nonmetal atoms (Figure 4).

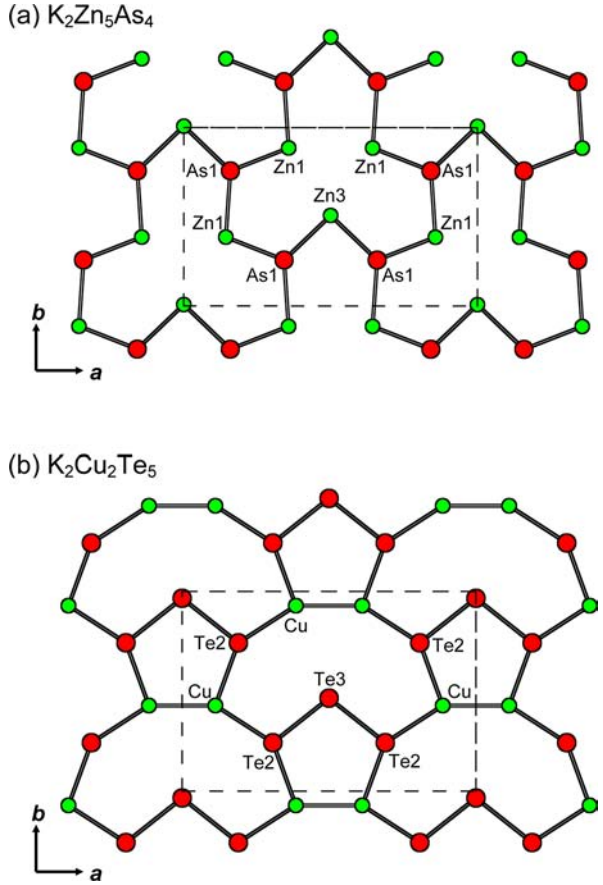


**Figure 4.** Comparison of nets parallel to the *ab*-plane present in (a) $K_2Zn_5As_4$ and (b) $K_2Cu_2Te_5$.

Inspection of interatomic distances (Table 3) indicates that the Zn−As contacts fall in the normal range (2.5−2.7 Å), the Zn−Zn contacts are probably too long to be bonding (3.0−3.1 Å), and As−As contacts are not present. Thus, these compounds are typical Zintl phases in which all atoms attain closed-shell electron configurations and charge balance is maintained: $(A^+)_2(Zn^{2+})_5(As^{3-})_4$. Band structure calculations on $K_2Zn_5As_4$ (Figure 5) confirm these expectations, with the

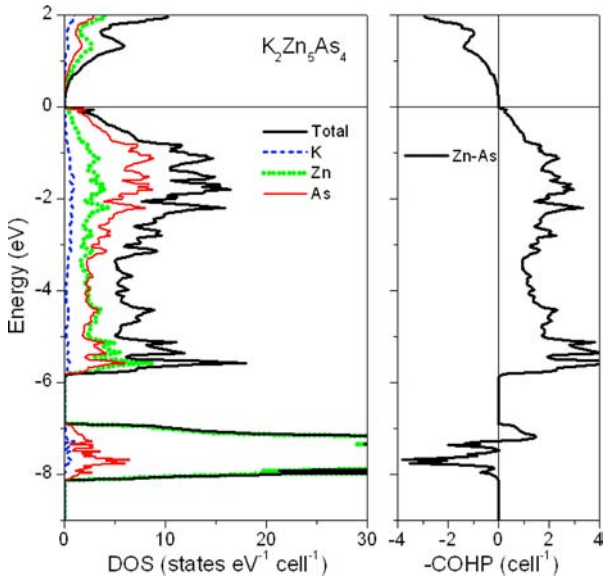


**Figure 5.** Density of states with atomic projections (left) and crystal orbital Hamilton population (COHP) curve for Zn−As contacts (right) in $K_2Zn_5As_4$. The horizontal line at 0 eV marks the Fermi level.

density of states (DOS) curve revealing nearly empty K-based states, completely filled Zn 3d states (the large spike between −7 and −8 eV), and nearly filled As-based states below the Fermi level. In fact, most of the bonding stability in the structure is derived from heteroatomic Zn−As contacts, which are perfectly optimized as seen by the occupation of all bonding and no antibonding levels in the crystal orbital Hamilton population (COHP) curve (Figure 5). These Zn−As bonds are strong (−ICOHP of 1.04 eV/bond and 12.5 eV/cell) and constitute >95% of the total covalent bonding energy in the structure, in contrast to the almost negligible contributions from K−As (−ICOHP of 0.02 eV/bond and 0.2 eV/cell) and Zn−Zn bonding (−ICOHP of 0.08 eV/bond and 0.3 eV/cell). The Zintl concept thus works well to account for the relatively minor role of the alkali-metal atoms as mere suppliers of electrons to the Zn−As framework, with the consequence that the analogous Rb-containing compound should also be expected to have a closely related electronic structure. Indeed, $K_2Zn_5As_4$ and $Rb_2Zn_5As_4$ have very similar band dispersion diagrams (Figure S3 in Supporting Information); both are predicted to be essentially direct band gap semiconductors with nearly the same gap energy of 0.4 eV between the valence and conduction bands.

## CONCLUSIONS

Adding to the growing family of ternary transition-metal arsenides, the compounds $A_2Zn_5As_4$ (A = K, Rb) exhibit a unique structure that can be described through *stellae quadrangulae* containing Zn-centered tetrahedra. They are likely amenable to substitution, not only through the obvious ones (e.g., Zn by Cd, or As by Sb),[18,24,25] but also through replacement with with a $d^5$ transition-metal component such as $Mn^{2+}$. Band structure calculations


dx.doi.org/10.1021/ic301311m | Inorg. Chem. 2012, 51, 9517−9521

on $K_2Zn_5As_4$ support the bonding picture implied by the Zintl concept: $K^+$ cations interact electrostatically with the anionic framework $[Zn_5As_4]^{2-}$, within which heteroatomic Zn−As covalent bonding predominates. If the modest air sensitivity of these compounds could be reduced, perhaps through appropriate chemical substitution of the alkali-metal component, it would be interesting to perform measurements of physical properties to determine if these compounds could be viable candidates for thermoelectric materials.

## ■ ASSOCIATED CONTENT

### Supporting Information

X-ray crystallographic files in CIF format, powder XRD patterns, an SEM image, and band dispersion diagrams. This material is available free of charge via the Internet at http://pubs.acs.org.

## ■ AUTHOR INFORMATION

### Corresponding Author

*E-mail: arthur.mar@ualberta.ca.

### Notes

The authors declare no competing financial interest.

## ■ ACKNOWLEDGMENTS

This work was supported by the Natural Sciences and Engineering Research Council of Canada.

## ■ REFERENCES

(1) Mandrus, D.; Sefat, A. S.; McGuire, M. A.; Sales, B. C. *Chem. Mater.* **2010**, *22*, 715−723.
(2) Eisenmann, B.; Cordier, G. In *Chemistry, Structure, and Bonding of Zintl Phases and Ions*; Kauzlarich, S. M., Ed.; VCH: New York, 1996; pp 61−137.
(3) Stoyko, S. S.; Mar, A. *J. Solid State Chem.* **2011**, *184*, 2360−2367.
(4) Stoyko, S. S.; Mar, A. *Inorg. Chem.* **2011**, *50*, 11152−11161.
(5) Nientiedt, A. T.; Lincke, H.; Rodewald, U. Ch.; Pöttgen, R.; Jeitschko, W. *Z. Naturforsch., B: J. Chem. Sci.* **2011**, *66*, 221−226.
(6) Hellman, A.; Löhken, A.; Wurth, A.; Mewis, A. *Z. Naturforsch., B: J. Chem. Sci.* **2007**, *62*, 155−161.
(7) Saparov, B.; Bobev, S. *Inorg. Chem.* **2010**, *49*, 5173−5179.
(8) Wilson, D. K.; Saparov, B.; Bobev, S. *Z. Anorg. Allg. Chem.* **2011**, *637*, 2018−2025.
(9) Stoyko, S. S.; Khatun, M.; Mar, A. *Inorg. Chem.* **2012**, *51*, 2621−2628.
(10) Nowotny, H.; Bachmeyer, K. *Monatsh. Chem.* **1949**, *8*, 734.
(11) Kuriyama, K.; Nakamura, F. *Phys. Rev. B* **1987**, *36*, 4439−4441.
(12) Kuriyama, K.; Kato, T.; Kawada, K. *Phys. Rev. B* **1994**, *49*, 11452−11455.
(13) Kalarasse, F.; Bennecer, B. *J. Phys. Chem. Solids* **2006**, *67*, 846−850.
(14) Nowotny, H.; Glatzl, B. *Monatsh. Chem.* **1951**, *82*, 720−722.
(15) Kahlert, H.; Schuster, H.-U. *Z. Naturforsch., B: Anorg. Chem., Org. Chem.* **1976**, *31*, 1538−1539.
(16) Jaganesh, G.; Merita Anto Britto, T.; Eithiraj, R. D.; Kalpana, G. *J. Phys.: Condens. Matter* **2008**, *20*, 085220−1−085220−8.
(17) Vogel, R.; Schuster, H.-U. *Z. Naturforsch., B: Anorg. Chem., Org. Chem.* **1980**, *35*, 114−116.
(18) He, H.; Tyson, C.; Bobev, S. *Inorg. Chem.* **2011**, *50*, 8375−8383.
(19) Prots, Yu.; Aydemir, U.; Öztürk, S. S.; Somer, M. *Z. Kristallogr.—New Cryst. Struct.* **2007**, *222*, 163−164.
(20) Deng, Z.; Jin, C. Q.; Liu, Q. Q.; Wang, X. C.; Zhu, J. L.; Feng, S. M.; Chen, L. C.; Yu, R. C.; Arguello, C.; Goko, T.; Ning, F.; Zhang, J.; Wang, Y.; Aczel, A. A.; Munsie, T.; Williams, T. J.; Luke, G. M.; Kakeshita, T.; Uchida, S.; Higemoto, W.; Ito, T. U.; Gu, B.; Maekawa, S.; Morris, G. D.; Uemura, Y. J. *Nat. Commun.* **2011**, *2*, 422.
(21) Sheldrick, G. M. *SHELXTL, version 6.12*; Bruker AXS Inc.: Madison, WI, 2001.
(22) Gelato, L. M.; Parthé, E. *J. Appl. Crystallogr.* **1987**, *20*, 139−143.
(23) Tank, R.; Jepsen, O.; Burkhardt, A.; Andersen, O. K. *TB-LMTO-ASA Program, version 4.7*; Max Planck Institut für Festkörperforschung: Stuttgart, Germany, 1998.
(24) Zheng, W.-Z.; Wang, P.; Wu, L.-M.; Liu, Y.; Chen, L. *Inorg. Chem.* **2010**, *49*, 5890−5896.
(25) Liu, Y.; Wu, L.-M.; Li, L.-H.; Du, S.-W.; Corbett, J. D.; Chen, L. *Angew. Chem., Int. Ed.* **2009**, *48*, 5305−5308.
(26) Nyman, H.; Andersson, S. *Acta Crystallogr., Sect. A* **1979**, *35*, 580−583.
(27) Nyman, H.; Andersson, S. *Acta Crystallogr., Sect. A* **1979**, *35*, 934−937.
(28) Nyman, H. *Acta Crystallogr., Sect. B* **1983**, *39*, 529−532.
(29) Zheng, C.; Hoffmann, R.; Nelson, D. R. *J. Am. Chem. Soc.* **1990**, *112*, 3784−3791.
(30) Häussermann, U.; Svensson, C.; Lidin, S. *J. Am. Chem. Soc.* **1998**, *120*, 3867−3880.
(31) Chen, X.; Huang, X.; Li, J. *Inorg. Chem.* **2001**, *40*, 1341−1346.